Inorganic Chemistry

Article

pubs.acs.org/IC

Inhomogeneous-Broadening-Induced Intense Upconversion Luminescence in Tm^{3+} and Yb^{3+} Codoped Lu_2O_3–ZrO_2 Disordered Crystals

Wen Liu,[†,‡] Zhendong Hao,[*,†] Liangliang Zhang,[†] Hao Wu,[†,‡] Xia Zhang,[†] Yongshi Luo,[†] Guohui Pan,[†] Haifeng Zhao,[†] Zuoling Fu,[§] and Jiahua Zhang[*,†]

[†]State Key Laboratory of Luminescence and Applications, Changchun Institute of Optics, Fine Mechanics and Physics, Chinese Academy of Sciences, 3888 Eastern South Lake Road, Changchun 130033, China

[‡]University of Chinese Academy of Sciences, Beijing 100049, China

[§]Coherent Light and Atomic and Molecular Spectroscopy Laboratory, Key Laboratory of Physics and Technology for Advanced Batteries, College of Physics, Jilin University, Changchun 130012, China

ABSTRACT: Near-infrared (980 nm) to near-infrared (800 nm) and blue (490 nm) upconversion has been studied in 0.2% Tm^{3+} and 10% Yb^{3+} codoped Lu_2O_3–ZrO_2 solid solutions as a function of the ZrO_2 content in the range of 0–50%, prepared by a high-temperature solid-state reaction. The continuous enhancement of upconversion luminescence is observed with increasing ZrO_2 content up to 30%. Analyses of the Yb^{3+} emission intensity and lifetime indicate enlarged absorption of a 980 nm excitation laser and enhanced energy transfer from Yb^{3+} to Tm^{3+} with the addition of ZrO_2. The spectrally inhomogeneous broadening of the dopants in this disordered solid solution is considered to play the main role in the enhancement by providing better matches with the excitation laser line and increasing the spectral overlap for efficient energy transfer from Yb^{3+} to Tm^{3+}. In addition, the inhomogeneous broadening is also validated to improve energy migration among Yb^{3+} ions and energy back transfer from Tm^{3+} to Yb^{3+}. Hence, it is understandable that a drop in the upconversion luminescence intensity occurs as the concentration of ZrO_2 is further increased from 30% to 50%. This work indicates the possibility of disordered crystals to achieve intense upconversion luminescence for biological and optoelectronic applications.

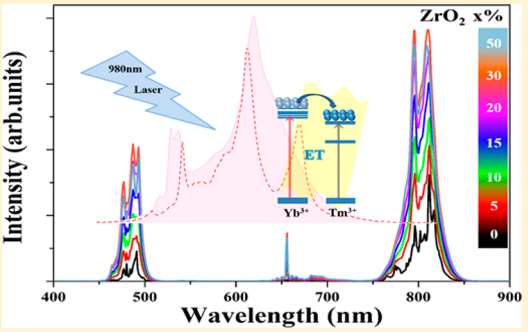

INTRODUCTION

Rare-earth-based upconversion (UC) materials have recently drawn considerable attention because of their potential applications in biolabeling, volumetric displays, solar cells, etc.[1−4] The selection of appropriate host materials is essential for highly efficient UC emissions.[5,6] To date, the most efficient host for UC is hexagonal $Na(Y,Lu)F_4$, but the toxicity of fluoride materials may greatly restrict their applicability in a variety of areas.[7−10] For this reason, UC in oxide materials is still significant because of their environmentally friendly and chemical-stable properties.[11] Oxides generally possess lower UC efficiency than fluorides because of their high phonon energies.[12] In this regard, methods to improve the UC intensities in oxides is imperative.

Cubic rare-earth sesquioxides Y_2O_3 and Lu_2O_3 have been widely adopted as the typical oxide UC hosts because of their relatively low phonon energy in oxides.[13−15] Compared with yttrium, lutetium is regarded as a more favorable cation for the emission of trivalent lanthanide dopants.[16] It is for this reason that the top of the valence band in Lu_2O_3 is mainly composed of Lu 4f orbitals rather than O or F 2p orbitals in Y_2O_3.[17] Lu_2O_3 has been reported as a proper host to obtain efficient upconversion luminescence (UCL) upon 980 nm laser-diode (LD) excitation when codoped with Tm^{3+}/Yb^{3+}, Er^{3+}/Yb^{3+}, and Ho^{3+}/Yb^{3+} couples.[18,19] Among these, the Tm^{3+}/Yb^{3+} combination is of particular interest because of its strong blue and near-IR (NIR) UC around 800 nm, which is located within the tissue optical transmission window (750–1000 nm).[20,21] Many kinds of techniques have been investigated to improve UCL in oxides, such as adjusting the dopant concentration, preparing the core/shell structure, etc.,[22−26] while achieving intense UC in disordered crystals is rarely mentioned.

Rare-earth sesquioxides and zirconia can form solid solutions, which are characterized by disordered crystals, because of which the absorption and luminescence spectra of rare-earth ions in these crystals demonstrate considerable inhomogeneous broadening[27]. Hence, the solid solution is a promising laser host for producing an ultrashort pulse laser and/or a wavelength-tunable laser.[28] If the solid solution is selected as the host for Yb^{3+}-sensitized UC, as in the case of ordered crystals, the pump wavelength only needs to simply fall within the broadened absorption band in the disordered crystals, instead of difficultly matching the narrow absorption line of Yb^{3+} in ordered crystals.

Received: July 10, 2017
Published: September 25, 2017

DOI: 10.1021/acs.inorgchem.7b01725
Inorg. Chem. 2017, 56, 12291−12296

The spectrally inhomogeneous broadening could make the absorption band of sensitizer Yb^{3+} easily match the 980 nm LD laser line and thus achieve intense UCL. To the best of our knowledge, UCL based on a sesquioxide $-ZrO_2$ system has not been reported yet.

In this paper, we report enhanced UCL of the Tm^{3+}/Yb^{3+} couple in Lu_2O_3 by the addition of ZrO_2 to form a $Lu_2O_3-ZrO_2$ solid solution. Compared with Lu_2O_3, the blue and NIR UCLs in a $Lu_2O_3-ZrO_2$ solid solution with 30% ZrO_2 are increased by 4.6 and 2.4 times, respectively. The role of spectrally inhomogeneous broadening of the dopants on the UCL enhancement is revealed, indicating enhanced absorption of the 980 nm LD line by Yb^{3+} and efficient energy transfer from Yb^{3+} to Tm^{3+} in $Lu_2O_3-ZrO_2$ disordered crystals. The mechanism for the improvement of UCL in the disordered crystals and the UC properties of a $Lu_2O_3-ZrO_2$ solid solution have been explained and demonstrated in detail.

EXPERIMENTAL SECTION

Sample Preparation. The series of samples investigated in this work were prepared by a solid-state reaction. The oxides Lu_2O_3 (4N), ZrO_2 (4N), Yb_2O_3 (4N), and Eu_2O_3 (4N) were employed as raw materials. The appropriate amount of Tm_2O_3 (4N) powder was dissolved in nitric acid to obtain a 0.005 M $Tm(NO_3)_3$ solution and then added into mixed oxides (Lu_2O_3, ZrO_2, and Yb_2O_3) with a corresponding mole ratio. The materials were mixed homogeneously by an agate mortar for 30 min, placed in a crucible with a lid, and then sintered at 1500 °C for 4 h to obtain the samples.

Spectroscopy Measurements. Powder X-ray diffraction (XRD) data were collected using Cu Kα radiation (λ = 1.54056 Å) on a Bruker D8 Advance diffractometer equipped with a linear position-sensitive detector (PSD-50m, M. Braun), operating at 40 kV and 40 mA with a step size of 0.01° (2θ) in the range of 10−80°. The steady-state excitation and emission spectra were measured using an FLS920 spectrometer (Edinburgh Instruments, Livingston, U.K.). A 980 nm LD was used to excite the Yb^{3+}:$^2F_{5/2}$ level, and an 808 nm LD was used for Tm^{3+}:$^3H_4$ solid-state excitation. In energy-level lifetime measurements, an OPO was used as an excitation source, and the signals were detected using a Tektronix digital oscilloscope (TDS 3052). The lifetimes were calculated as integration of the area under the corresponding decay curves with normalized initial intensity. All of the measurements above were performed at room temperature.

RESULTS AND DISCUSSION

Figure 1 shows the XRD patterns of 0.2% Tm_2O_3−10% Yb_2O_3−(89.8 − x)% Lu_2O_3−x% ZrO_2 powder samples with x = 0, 5, 10, 15, 20, 30, and 50. The main diffraction peaks are exclusively displayed in order to clearly present their positions and shapes. The XRD patterns can be well indexed to cubic Lu_2O_3 (PDF 12-0728) for ZrO_2-free and $Lu_4Zr_3O_{12}$ (PDF 77-0738) for 50% ZrO_2. In Figure 1, the asterisk symbol represents for the Lu_2O_3 phase and the triangle symbol indicates the $Lu_4Zr_3O_{12}$ phase. The evolution of the two phases can be clearly shown in the enlarged main peak for (222) in the right column of Figure 1. The addition of ZrO_2 leads to the main diffraction peak of Lu_2O_3 shifting toward high angles until the ZrO_2 content reached up to 30%, which indicates the substitution of Lu^{3+} ions (with a radius of 0.977 Å) by Zr^{4+} ions (0.720 Å), with the smaller ionic radius causing the host lattice to shrink. One observes that a shoulder appears at the high-angle side of the main peak for a ZrO_2 content of ≥15% and the shoulder grows with increasing ZrO_2 content. At 50% ZrO_2, the shoulder becomes a main peak, which is assigned to the $Lu_4Zr_3O_{12}$ phase.

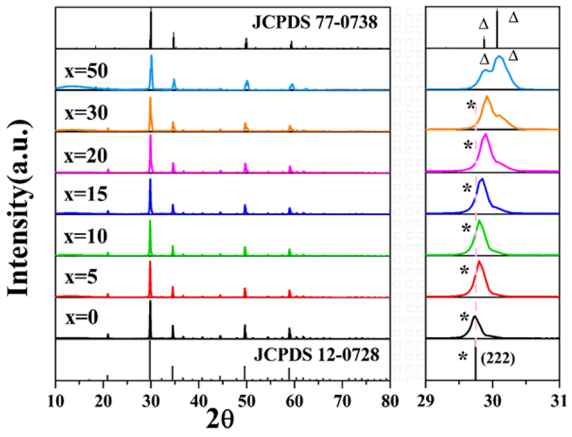

Figure 1. XRD patterns of 0.2% Tm^{3+}/10% Yb^{3+}/(89.8 − x)% Lu_2O_3/x% ZrO_2 (x = 0−50) and the standard XRD data of Lu_2O_3 (JCPDS 12-0728) and $Lu_4Zr_3O_{12}$ (JCPDS 77-0738). The right column is the partially enlarged detail of the (222) peak.

Figure 2 exhibits the UC emission spectra of the samples upon 980 nm LD excitation. Three distinct UC emission bands

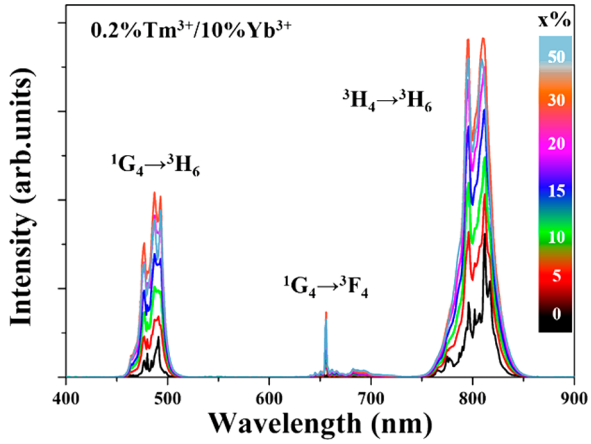

Figure 2. UCL spectra of 0.2% Tm^{3+}/10% Yb^{3+}/(89.8 − x)% Lu_2O_3/x % ZrO_2 (x = 0, 5, 10, 15, 20, 30, and 50) under 980 nm excitation at room temperature.

in the range of 400−900 nm are observed. The blue emission peaking at around 490 nm and the red emission peaking at 655 nm are assigned to the transitions of Tm^{3+} from $^1G_4$ to $^3H_6$ and $^3F_4$, respectively. The strong NIR band around 800 nm originated from the Tm^{3+}:$^3H_4$ → $^3H_6$ transition. It is observed that the UC emissions have pronounced enhancement with increasing composition of ZrO_2 up to 30%, above which the UCL starts to decrease. Compared with Lu_2O_3, the blue and NIR UC emissions for 30% ZrO_2 are enhanced by factors of 4.6 and 2.4, respectively. Energy transfer from Yb^{3+} to Tm^{3+} is studied based on the energy transfer of the UC model for the Tm^{3+}/Yb^{3+} system, as shown in Figure 3. Yb^{3+} acts as an efficient sensitizer, which has a large absorption cross section at 980 nm and a long $^2F_{5/2}$ state lifetime.[29] Under 980 nm excitation, the $^2F_{5/2}$ level of Yb^{3+} is populated, and subsequently the excited Yb^{3+} carries out step energy transfer to Tm^{3+} to produce UCL.

In order to understand the origin of the UC enhancement, the effectiveness of Yb^{3+} excitation by a 980 nm LD and the efficiency of energy transfer from Yb^{3+} to Tm^{3+} are studied for

DOI: 10.1021/acs.inorgchem.7b01725
Inorg. Chem. 2017, 56, 12291−12296

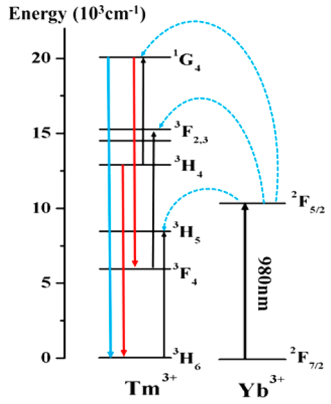

Figure 3. Schematic energy-level diagram and mechanism of the UC process in a Tm^{3+}/Yb^{3+} codoped system following excitation with 980 nm.

different ZrO_2 contents. Figure 4 presents the emission spectra of 10% Yb^{3+} singly doped and 0.2% Tm^{3+}/10% Yb^{3+} codoped

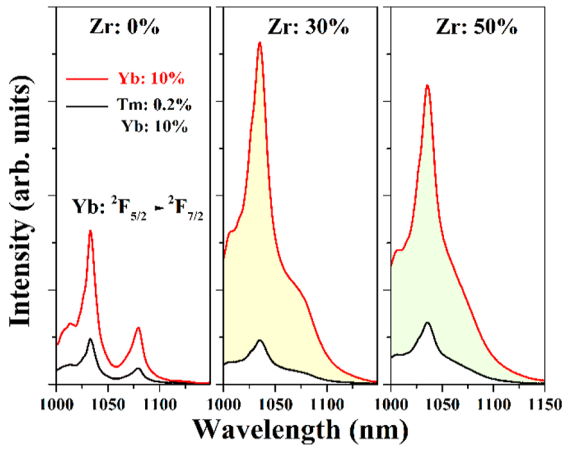

Figure 4. Comparison of the IR emission spectra of Yb^{3+} singly doped and Tm^{3+}/Yb^{3+} codoped Lu_2O_3–ZrO_2 (x = 0, 30, and 50) samples excited by a 980 nm LD. The red line stands for single doping with 10% Yb^{3+}, and the black line represents 0.2% Tm^{3+}/10% Yb^{3+} codoped samples.

Lu_2O_3–ZrO_2 solid solutions for different ZrO_2 contents (x = 0, 30, and 50) under 980 nm excitation. In the Yb^{3+} singly doped situation, the strong peaks of three samples at 1035 nm are assigned to the Yb^{3+}:$^2F_{5/2}$ → $^2F_{7/2}$ transition. It is clearly displayed in Figure 4 that the emission band of Yb^{3+} is strikingly broadened with the addition of ZrO_2 because of the increase of disordered structure in a Lu_2O_3–ZrO_2 solid solution. The integrated intensity of 10% Yb^{3+} emission for 30% ZrO_2 is the strongest of the three samples. When 0.2% Tm^{3+} is codoped, the Yb^{3+} emission intensities fall sharply in all samples because of effective energy transfer from Yb^{3+} to Tm^{3+}. It is clear that the fraction of the decrement becomes larger with increasing ZrO_2 concentration, indicating more efficient energy transfer in this system. The efficient energy transfer is also supported by the lifetime shortening of the Yb^{3+} emission in the presence of Tm^{3+}.

It is shown in Figure 5 that the decay curves of Yb^{3+} emission for 0.2% Yb^{3+} singly doped, 10% Yb^{3+} singly doped, and 0.2% $Tm^{3+}/10\%$ Yb^{3+} codoped samples with ZrO_2 free (a), 30% ZrO_2 (b), and 50% ZrO_2 (c). From Figure 5, the lifetimes of

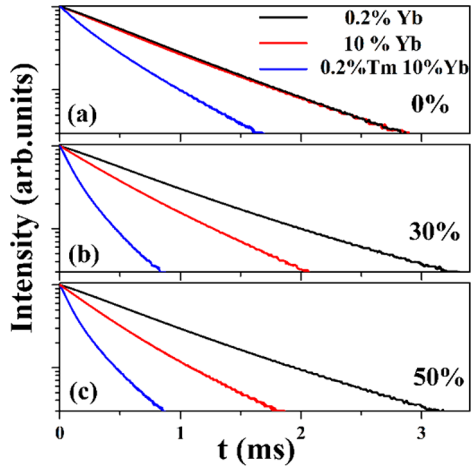

Figure 5. Decay curves of the Yb^{3+} emission in Lu_2O_3–ZrO_2 doped with 0.2% Yb or 10% Yb or codoped 0.2% Tm and 10% Yb for different ZrO_2 contents after 980 nm pulse excitation.

0.2% Yb^{3+} lowly doped samples with different ZrO_2 contents are close to each other, indicating their comparable intrinsic lifetimes (τ_i) or radiative lifetimes. The emission lifetimes of Yb^{3+} for singly doped samples, 0.2% Yb^{3+} (τ_i), 10% Yb^{3+} (τ_0), and 0.2% $Tm^{3+}/10\%$ Yb^{3+} codoped samples (τ), are calculated from the area under the corresponding decay curves with a normalized initial intensity, as listed in Table 1. With an

Table 1. Emission Lifetimes, Emission Intensities (I), Emission Efficiencies (η_E), Absorbance (η_{Abs}) of Yb^{3+}, and Efficiencies (η_{ET}) of Energy Transfer from Yb^{3+} to Tm^{3+} in a Lu_2O_3–ZrO_2 System

	0.2% Yb^{3+}		10% Yb^{3+}			0.2% Tm^{3+}/ 10% Yb^{3+}	
ZrO_2 content (%)	τ_i (μs)	I	τ_0 (μs)	η_E	η_{Abs}	τ (μs)	η_{ET}
0	801	0.45	772	0.96	0.31	409	0.47
30	860	1	534	0.62	1	193	0.64
50	846	0.88	458	0.54	1.01	190	0.59

increase of the singly doped Yb^{3+} concentration from 0.2% to 10%, the lifetime is slightly shortened for the ZrO_2-free sample, whereas it is markedly shortened for 30% ZrO_2 and 50% ZrO_2. The less changed lifetime for the ZrO_2-free sample is attributed to ineffective energy migration among Yb^{3+} ions due to nearly no distortion in the Lu_2O_3 crystal structure when doped with Yb^{3+}, which has almost the same radius as Lu^{3+}. The lifetime shortening in the presence of ZrO_2 is originated from effective energy migration among Yb^{3+} ions. Energy migration is caused by an increase of spectral overlap between Yb^{3+} ions under the condition of spectrally inhomogeneous broadening in the disordered crystals. The lifetime shortening implies a reduction of the emission efficiency, which can be calculated by $\eta_E = \tau_0/\tau_i$. However, the samples with 30% and 50% ZrO_2 present stronger Yb^{3+} emissions than Lu_2O_3. It is known that the fluorescence intensity is proportional to the product of the absorbance and emission efficiency. Therefore, it indicates that the absorption of 980 nm excitation by Yb^{3+} in the presence of ZrO_2 is enhanced. This result is explained by the fact that the 980 nm laser hardly well matches the sharp Yb^{3+} absorption line in Lu_2O_3 but easily falls within the broadened Yb^{3+} absorption band in the disordered Lu_2O_3–ZrO_2 crystals. In

DOI: 10.1021/acs.inorgchem.7b01725
Inorg. Chem. 2017, 56, 12291–12296

addition, if the emission intensity and absorbance of the 30% ZrO_2 sample are defined as 1, the absorbance of the series could be evaluated. The Yb^{3+} emission intensity for 50% ZrO_2 is 88% that for 30% ZrO_2, while the emission efficiency of Yb^{3+} for 50% ZrO_2 (54%) is 87% that for 30% ZrO_2 (62%). This implies that the absorbance of 980 nm excitation for 50% ZrO_2 is 88/87% that for 30% ZrO_2. Hence, it can be concluded that the absorbance of 980 nm excitation by Yb^{3+} ions improves with increasing ZrO_2 content in a Lu_2O_3–ZrO_2 solid solution. Upon codoping with Tm^{3+} and Yb^{3+}, the shortened lifetimes are mainly attributed to the first step energy transfer from Yb^{3+}:$^2F_{5/2}$ to Tm^{3+}:$^3F_4$ under Yb:$^2F_{5/2}$ direct excitation at 980 nm. The efficiency (η_{ET}) of energy transfer from Yb^{3+} to Tm^{3+} is calculated by $\eta_{ET} = 1 - \tau/\tau_0$. The calculated transfer efficiency for 30% ZrO_2 is 0.64, which is the highest one among the three samples. This result is in accordance with the emission spectra of Yb^{3+}, shown in Figure 4.

All of the results indicated above can be well attributed to the effect of spectrally inhomogeneous broadening of the dopants in a Lu_2O_3–ZrO_2 solid solution. The inhomogeneous broadening can not only make the absorption band of Yb^{3+} match the 980 nm laser line better but also increase the spectral overlap between dopants for efficient energy transfer. The emission lifetime shortening of Yb^{3+} with increasing ZrO_2 content for Yb^{3+} single doping can be explained as continuously enhanced energy transfer between Yb^{3+} ions due to a continuous increase of the structure disorder with increasing ZrO_2 content up to 50%. The enhanced energy transfer between Yb^{3+} ions thus speeds up excitation energy loss to quenchers. It is then understandable why the most efficient energy transfer from Yb^{3+} to Tm^{3+} occurs at 30% ZrO_2 rather than 50% ZrO_2, for which efficient energy transfer between Yb^{3+} ions strongly suppresses energy transfer to Tm^{3+}.

The disordered structures can be further proven by the observed emission band broadening of Yb^{3+} with the addition of ZrO_2 in a Lu_2O_3–ZrO_2 solid solution, as shown in Figure 6.

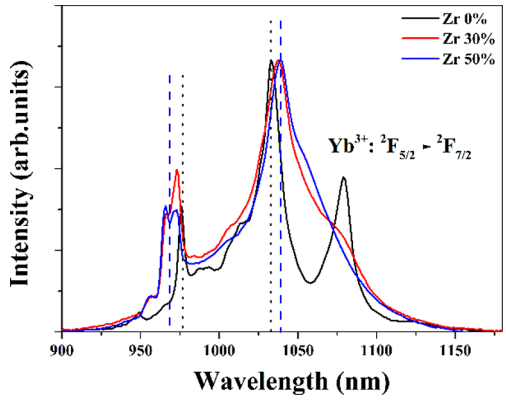

Figure 6. IR emission spectra of 0.2% Tm_2O_3/10% Yb_2O_3/(89.8 − x)% Lu_2O_3/x% ZrO_2 (x = 0, 30, and 50) samples excited by a 808 nm LD. The spectra are normalized with a maximum emission intensity at around 1040 nm.

The emission shape of Yb^{3+} is measured upon Tm^{3+}:$^3H_4$ excitation at 808 nm because there exists energy back transfer from Tm^{3+} in the $^3H_4$ state to Yb^{3+} in the ground state[30] to get rid of the influence from a 980 nm laser. The spectra are normalized with the maximum emission intensity to clarify the spectral shifts. With increasing the ZrO_2 content, the shift is as large as 15 nm, depicted by the dashed and dotted lines in Figure 6. We also find that the Stark energy splitting of the Yb^{3+} emission is growing larger, followed by enhanced inhomogeneous broadening. The enhanced Stark energy splitting is attributed to the fact that introducing ZrO_2 shortens the average bond length and thus strengthens the crystal field acting on the Yb^{3+} ions. As to the improved inhomogeneous broadening of Yb^{3+} emission, this is due to the enhanced disordered structure in a Lu_2O_3–ZrO_2 solid solution.[31] The broadening of the Yb^{3+} emission is beneficial to the spectral overlap between Yb^{3+}:$^2F_{5/2}$–$^2F_{7/2}$ emission and Tm^{3+}:$^3H_6$–$^3H_5$ absorption, thus elevating the efficiency of energy transfer from Yb^{3+} to Tm^{3+} in the ground state. One may wonder why the transfer efficiency for 50% ZrO_2 is lower than that for 30% ZrO_2. This may be related to their ability of energy back transfer.

With regard to the decrease of UCL for 50% ZrO_2 compared to 30% ZrO_2, deexcitation of Tm^{3+}:$^3H_4$ due to energy back transfer to Yb^{3+} is also examined. Figure 7 shows the

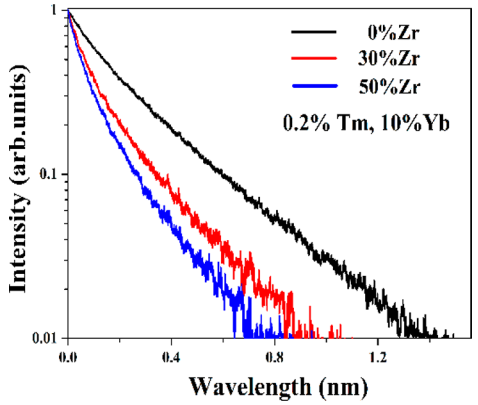

Figure 7. Fluorescence decay curves when monitoring the Tm^{3+}:$^3H_4$ state in 0.2% Tm_2O_3/10% Yb_2O_3/(89.8 − x)% Lu_2O_3/x% ZrO_2 samples (x = 0, 30, and 50).

fluorescence decay curves of the Tm^{3+}:$^3H_4$ level for different ZrO_2 contents after pulse excitation of the Tm^{3+}:$^3F_{2,3}$ state at 690 nm. This shows that the $^3H_4$ lifetimes are continuously shortened with increasing ZrO_2 content, denoting a continuously enhanced energy back transfer.

Therefore, it is considered that although the Stark energy splitting of the 50% ZrO_2 sample is larger than that of the 30% ZrO_2 one, more effective energy back transfer from Tm^{3+} to Yb^{3+} may offset the effects of $Yb^{3+} \rightarrow Tm^{3+}$ energy transfer and decrease the UCL intensity. Efficient energy back transfer for 50% ZrO_2 is also observed in photoluminescence spectra.

Figure 8 shows NIR emission spectra of Tm^{3+} singly doped and Tm^{3+}/Yb^{3+} codoped samples upon Tm^{3+}:$^3H_4$ excitation at 808 nm. The group of emission lines at around 1400 nm are attributed to a Tm^{3+}:$^3H_4 \rightarrow {}^3F_4$ transition. The band peaking at 1620 nm is a small amount of the Tm^{3+}:$^3F_4 \rightarrow {}^3H_6$ emission, which achieves the strongest peak at around 2 μm. The wavelength beyond 1620 nm is undetected because of the cutoff wavelength at 1650 nm of the InGaAs detector used in this work. The red lines represent Tm^{3+} and Yb^{3+} codoped samples, and the black lines stand for Tm^{3+} singly doped ones. Yb^{3+}:$^2F_{5/2} \rightarrow {}^2F_{7/2}$ emission in the range of 900–1100 nm is a result of energy back transfer from Tm^{3+}:$^3H_4$ to Yb^{3+}:$^2F_{5/2}$. For a clear comparison of the emission spectra, the codoped and singly doped samples with the same ZrO_2 content are plotted together, where the $^3H_4 \rightarrow {}^3F_4$ emission intensity for the singly

DOI: 10.1021/acs.inorgchem.7b01725
Inorg. Chem. 2017, 56, 12291–12296

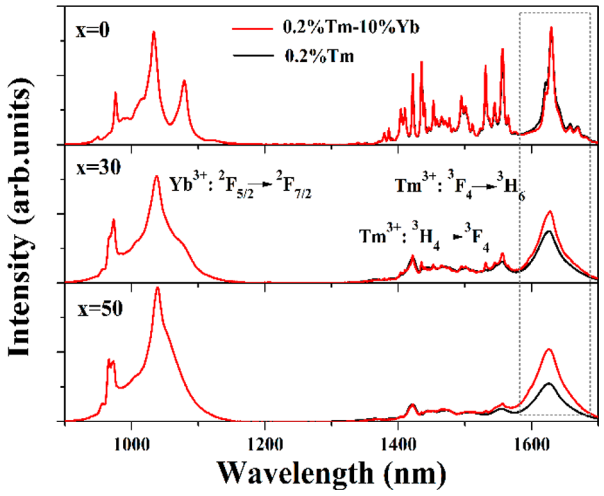

Figure 8. Comparison of IR emission spectra in 0.2% Tm_2O_3/10% Yb_2O_3/(89.8 − x)% Lu_2O_3/x% ZrO_2 and 0.2% Tm_2O_3/(99.8 − x)% Lu_2O_3/x% ZrO_2 (x = 0, 30, and 50) samples under 808 nm excitation.

doped sample is scaled to that for the codoped sample. The appearance of Yb^{3+} emission upon Tm^{3+}:$^3H_4$ excitation can directly prove energy transfer from Tm^{3+}:$^3H_4$ to Yb^{3+}:$^2F_{5/2}$. It is noticed that there is a decrease in the 1400 nm emission band when the ZrO_2 content is increased. Besides that, the $^3F_4 \rightarrow {}^3H_6$ emission intensity becomes much stronger than the singly doped one with increasing ZrO_2 content, especially for the 50% ZrO_2 sample. These phenomena can be well explained as follows:[32] Under 808 nm excitation, the $^3H_4$ excited state of Tm^{3+} is populated. A Tm^{3+} ion in the $^3H_4$ excited state tends to transfer energy to a nearby Yb^{3+} ion, leading to a decrease of the Tm^{3+} emission from $^3H_4$ and generation of the Yb^{3+} emission. Subsequently, the excited Yb^{3+} transfers its energy to Tm^{3+} again to promote population of the Tm^{3+}:$^3F_4$ state, thus enhancing the Tm^{3+}:$^3F_4 \rightarrow {}^3H_6$ emission. Besides this process, this $^3H_4$ population could also relax to the $^3F_4$ level by $^3H_4 \rightarrow {}^3F_4$, $^3H_5$ radiative transitions and cascade MPR through the $^3H_5$ state. When energy transfer from Tm^{3+} to Yb^{3+} is dominant, the $^3H_4 \rightarrow {}^3F_4$ emission will accordingly decrease. In this situation, the $^3H_4 \rightarrow {}^3H_6$ emission is assigned to the energy back transfer. This process is presented in Figure 9. Therefore, the smaller ratio of Tm^{3+}:$^3H_4 \rightarrow {}^3F_4$ to the $^3F_4 \rightarrow {}^3H_6$ emission is direct evidence of increasing energy back transfer. In addition, when the increments of the Tm^{3+}:$^3F_4 \rightarrow {}^3H_6$ emission for different ZrO_2 contents are compared, it could also be demonstrated that the sample with 50% ZrO_2 has the most efficient energy back transfer, resulting in a decrease of the UC emission at 800 nm. This conclusion is in accordance with the $^3H_4$ decay features shown in Figure 7.

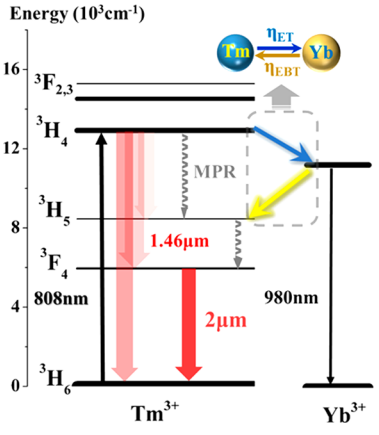

Figure 9. Schematic energy level diagram and energy back transfer process in Lu_2O_3−ZrO_2 disordered crystals.

The dependence of the UC emission intensity on the pump power is measured to better illustrate the populated states for visible and NIR UC emissions. As to an unsaturated UC process, the number of photons (n) required to populate the corresponding states could be determined from the slope in a double-logarithmic diagram, as shown in Figure 10. According to $I \propto P^n$, where the UCL intensity (I) is proportional to the nth power (P) under low excitation.[33] By variation of the incident pump power of a 980 nm LD, the NIR and visible emission intensities in 0.2% Tm_2O_3/10% Yb_2O_3/59.8% Lu_2O_3/30% ZrO_2 have been fit with two straight lines with slopes of 1.86 and 2.70, respectively. This confirms that the NIR emission from the Tm^{3+}:$^3H_4 \rightarrow {}^3H_6$ transition is a two-photon process and the blue emission ascribed to the Tm^{3+}:$^1G_4 \rightarrow {}^3H_6$ transition required three photons to be achieved.

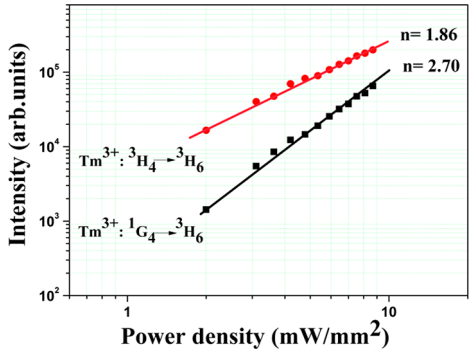

Figure 10. Pump power dependence of the emission intensity from the $^3H_4$ and $^1G_4$ excited states in a Tm^{3+}/Yb^{3+} codoped 30% ZrO_2 sample under 980 nm LD excitation.

CONCLUSIONS

In summary, a Lu_2O_3−ZrO_2 UC system has been successfully achieved, and the UC properties have been first investigated. Upon codoping with Tm^{3+} and Yb^{3+}, upon 980 nm excitation, the visible and NIR UC emission intensities are significantly enhanced by the addition of ZrO_2. The blue and NIR luminescences of a 30% ZrO_2 sample are improved by 4.6- and 2.4-fold compared with Lu_2O_3. This enhancement should be attributed to the inhomogeneous broadening of the dopants in this disordered solid solution, which is conducive to well fitting with the excitation laser line and promoting the energy-transfer process. Meanwhile, the increasing energy back transfer that leads to the decline in UCL of a 50% ZrO_2 sample has also been discussed. These investigations provide the possibility of disordered crystals being utilized as a UC system, which may be beneficial to achieving practical applications.

AUTHOR INFORMATION

Corresponding Authors

*E-mail: haozd@ciomp.ac.cn. Tel./Fax: +86-431-8617-6317.
*E-mail: zhangjh@ciomp.ac.cn. Tel./Fax: +86-431-8617-6317.

ORCID

Wen Liu: 0000-0001-5792-6830

DOI: 10.1021/acs.inorgchem.7b01725
Inorg. Chem. 2017, 56, 12291−12296

Notes

The authors declare no competing financial interest.

■ ACKNOWLEDGMENTS

This work was supported by the National Key R&D Program of China (Grants 2016YFB0701003 and 2016YFB0400605), the National Natural Science Foundation of China (Grants 61275055, 11274007, 51402284, and 11604330), the Natural Science Foundation of Jilin Province (Grants 20140101169JC, 20150520022JH, and 2525220160520171JH), and the State Key Laboratory of Luminescence and Applications.

■ REFERENCES

(1) Liu, Q.; Feng, W.; Yang, T.; Yi, T.; Li, F. Upconversion luminescence imaging of cells and small animals. *Nat. Protoc.* **2013**, *8*, 2033−2044.

(2) Wang, F.; Liu, X. G. Upconversion multicolor fine-tuning: visible to near-infrared emission from lanthanide-doped NaYF4 nanoparticles. *J. Am. Chem. Soc.* **2008**, *130*, 5642−5643.

(3) Van der Ende, B. M.; Aarts, L.; Meijerink, A. Lanthanide ions as spectral converters for solar cells. *Phys. Chem. Chem. Phys.* **2009**, *11*, 11081−11095.

(4) Liu, K.; Zhang, Z.; Shan, C.; Feng, Z.; Li, J.; Song, C.; Bao, Y.; Qi, X.; Dong, B. A flexible and superhydrophobic upconversion-luminescence membrane as an ultrasensitive fluorescence sensor for single droplet detection. *Light: Sci. Appl.* **2016**, *5*, e16136.

(5) Li, X.; Wang, R.; Zhang, F.; Zhao, D. Engineering homogeneous doping in single nanoparticle to enhance upconversion efficiency. *Nano Lett.* **2014**, *14*, 3634.

(6) Wang, F.; Liu, X. Recent advances in the chemistry of lanthanide-doped upconversion nanocrystals. *Chem. Soc. Rev.* **2009**, *38*, 976−989.

(7) Heer, S.; Kompe, K.; Güdel, H. U.; Haase, M. Highly efficient multicolour upconversion emission in transparent colloids of lanthanide-doped $NaYF_4$ nanocrystals. *Adv. Mater.* **2004**, *16*, 2102.

(8) Zeng, S. J.; Xiao, J. J.; Yang, Q. B.; Hao, J. H. Bi-functional $NaLuF_4$: $Gd^{3+}/Yb^{3+}/Tm^{3+}$ nanocrystals: structure controlled synthesis, near-infrared upconversion emission and tunable magnetic properties. *J. Mater. Chem.* **2012**, *22*, 9870.

(9) Dong, B.; Cao, B. S.; He, Y. Y.; Liu, Z.; Li, Z. P.; Feng, Z. Q. Temperature sensing and in vivo imaging by molybdenum sensitized visible upconversion luminescence of rare-earth oxides. *Adv. Mater.* **2012**, *24*, 1987−1993.

(10) Etchart, I.; Hernández, I.; Huignard, A.; Bérard, M.; Gillin, W. P.; Curry, R. J.; Cheetham, A. K. Efficient oxide phosphors for light upconversion; green emission from Yb^{3+} and Ho^{3+} co-doped Ln_2BaZnO_5 (Ln= Y, Gd). *J. Mater. Chem.* **2011**, *21*, 1387.

(11) Capobianco, J. A.; Vetrone, F.; Boyer, J. C.; Speghini, A.; Bettinelli, M. Enhancement of red emission ($^4F_{9/2}\rightarrow{}^4I_{15/2}$) via upconversion in bulk and nanocrystalline cubic Y_2O_3: Er^{3+}. *J. Phys. Chem. B* **2002**, *106*, 1181−1187.

(12) Li, Z. P.; Dong, B.; He, Y. Y.; Cao, B. S.; Feng, Z. Q. Selective enhancement of green upconversion emissions of Er^{3+}: $Yb_3Al_5O_{12}$ nanocrystals by high excited state energy transfer with $Yb^{3+}-Mn^{2+}$ dimer sensitizing. *J. Lumin.* **2012**, *132*, 1646.

(13) Zhang, F.; Braun, G. B.; Shi, Y. F.; Zhang, Y. C.; Sun, X. H.; Reich, N. O.; Zhao, D. Y.; Stucky, G. Fabrication of $Ag@SiO_2@Y_2O_3$: Er nanostructures for bioimaging: tuning of the upconversion fluorescence with silver nanoparticles. *J. Am. Chem. Soc.* **2010**, *132*, 2850.

(14) Yang, J.; Zhang, C. M.; Peng, C.; Li, C. X.; Wang, L. L.; Chai, R. T.; Lin, J. Controllable red, green, blue (RGB) and bright white upconversion luminescence of Lu_2O_3: $Yb^{3+}/Er^{3+}/Tm^{3+}$ nanocrystals through single laser excitation at 980 nm. *Chem. - Eur. J.* **2009**, *15*, 4649−4655.

(15) Zhang, J. H.; Hao, Z. D.; Li, J.; Zhang, X.; Luo, Y. S.; Pan, G. H. Observation of efficient population of the red-emitting state from the green state by non-multiphonon relaxation in the $Er^{3+}-Yb^{3+}$ system. *Light: Sci. Appl.* **2015**, *4*, e239.

(16) Li, L.; Zhang, X.; Wei, X.; Wang, G.; Guo, C. Near-Infrared to visible upconversion in Tm^{3+} and Yb^{3+} codoped Lu_2O_3 nanocrystals synthesized by hydrothermal method. *J. Nanosci. Nanotechnol.* **2014**, *14*, 4313−4319.

(17) Vetrone, F.; Boyer, J. C.; Capobianco, J. A.; Speghini, A.; Bettinelli, M. NIR to visible upconversion in nanocrystalline and bulk Lu_2O_3: Er^{3+}. *J. Phys. Chem. B* **2002**, *106*, 5622.

(18) An, L. Q.; Zhang, J.; Liu, M.; Wang, S. W. Preparation and upconversion properties of Yb^{3+}, Ho^{3+}: Lu_2O_3 nanocrystalline powders. *J. Am. Ceram. Soc.* **2005**, *88*, 1010.

(19) Li, Y.; Zhang, J.; Zhang, X.; Luo, Y.; Ren, X.; Zhao, H.; Wang, X.; Sun, L.; Yan, C. Near-infrared to visible upconversion in Er^{3+} and Yb^{3+} codoped Lu_2O_3 nanocrystals: enhanced red color upconversion and three-photon process in green color upconversion. *J. Phys. Chem. C* **2009**, *113*, 4413−4418.

(20) Nyk, M.; Kumar, R.; Ohulchanskyy, T. Y.; Bergey, E. J.; Prasad, P. N. High contrast in vitro and in vivo photoluminescence bioimaging using near infrared to near infrared up-conversion in Tm^{3+} and Yb^{3+} doped fluoride nanophosphors. *Nano Lett.* **2008**, *8*, 3834−3838.

(21) Yu, D. C.; Martin-Rodriguez, R.; Zhang, Q. Y.; Meijerink, A.; Rabouw, F. T. Multi-photon quantum cutting in Gd_2O_2S: Tm^{3+} to enhance the photo-response of solar cells. *Light: Sci. Appl.* **2015**, *4*, e344.

(22) Li, Y. P.; Zhang, J. H.; Luo, Y. S.; Zhang, X.; Hao, Z. D.; Wang, X. J. Color control and white light generation of upconversion luminescence by operating dopant concentrations and pump densities in Yb^{3+}, Er^{3+} and Tm^{3+} tri-doped Lu_2O_3 nanocrystals. *J. Mater. Chem.* **2011**, *21*, 2895.

(23) Chen, G.; Liu, H.; Liang, H.; Somesfalean, G.; Zhang, Z. Upconversion emission enhancement in Yb^{3+}/Er^{3+}-codoped Y_2O_3 nanocrystals by tridoping with Li^+ ions. *J. Phys. Chem. C* **2008**, *112*, 12030.

(24) Capobianco, J. A.; Vetrone, F.; Boyer, J. C.; Speghini, A.; Bettinelli, M. Enhancement of red emission ($^4F_{9/2}\rightarrow{}^4I_{15/2}$) via upconversion in bulk and nanocrystalline cubic Y_2O_3: Er^{3+}. *J. Phys. Chem. B* **2002**, *106*, 1181−1187.

(25) Jia, G.; You, H.; Song, Y.; Huang, Y.; Yang, M.; Zhang, H. Facile synthesis and luminescence of uniform Y_2O_3 hollow spheres by a sacrificial template route. *Inorg. Chem.* **2010**, *49*, 7721.

(26) Pandey, A.; Rai, V. K. Improved luminescence and temperature sensing performance of $Ho^{3+}-Yb^{3+}-Zn^{2+}$: Y_2O_3 phosphor. *Dalton Trans.* **2013**, *42*, 11005.

(27) Voron'ko, Y. K.; Sobol', A. A.; Ushakov, S. N.; Shukshin, V. E. Spectroscopy of disordered laser crystals. *Inorg. Mater.* **2002**, *38*, 390−396.

(28) Borik, M. A.; Lomonova, E. E.; Malov, A. V.; Kulebyakin, A. V.; Ryabochkina, P. A.; Ushakov, S. N.; Uslamina, M. A.; Chabushkin, A. N. Spectral, luminescent, and lasing properties of ZrO_2—Y_2O_3—Tm_2O_3 crystals. *Quantum Electron.* **2012**, *42*, 580−582.

(29) Zheng, K.; Zhang, D.; Zhao, D.; Liu, N.; Shi, F.; Qin, W. Bright white upconversion emission from Yb^{3+}, Er^{3+}, and Tm^{3+}-codoped Gd_2O_3 nanotubes. *Phys. Chem. Chem. Phys.* **2010**, *12*, 7620.

(30) Huang, L.; Shen, S.; Jha, A. Near infrared spectroscopic investigation of $Tm^{3+}-Yb^{3+}$ co-doped tellurite glasses. *J. Non-Cryst. Solids* **2004**, *345−346*, 349−353.

(31) Xu, Z.; He, L.; Mu, R.; Zhong, X.; Zhang, Y.; Zhang, J.; Cao, X. Double-ceramic-layer thermal barrier coatings of $La_2Zr_2O_7$/YSZ deposited by electron beam-physical vapor deposition. *J. Alloys Compd.* **2009**, *473*, 509−515.

(32) Liu, W.; Hao, Z.; Zhang, L.; Zhang, X.; Luo, Y.; Pan, G.; Wu, H.; Zhang, J. Enhanced $^3H_4$-$^3F_4$ nonradiative relaxation of Tm^{3+} through energy transfer to Yb^{3+} and efficient back transfer in lowly Tm^{3+} doped $Lu_{1.6}Sc_{0.4}O_3$: Tm^{3+}, Yb^{3+}. *J. Alloys Compd.* **2017**, *696*, 627−631.

(33) Strek, W.; Cichy, B.; Radosinski, L.; Gluchowski, P.; Marciniak, L.; Lukaszewicz, M.; Hreniak, D. Laser-induced white-light emission from graphene ceramics−opening a band gap in graphene. *Light: Sci. Appl.* **2015**, *4*, e237.

DOI: 10.1021/acs.inorgchem.7b01725
Inorg. Chem. 2017, 56, 12291−12296